ACS Catalysis

pubs.acs.org/acscatalysis

Research Article

One-Pot Asymmetric Synthesis of an Aminodiol Intermediate of Florfenicol Using Engineered Transketolase and Transaminase

Qi Liu, Xinyue Xie, Mancheng Tang, Wentao Tao, Ting Shi, Yuanzhen Zhang, Tingting Huang, Yilei Zhao, Zixin Deng, and Shuangjun Lin*

Cite This: *ACS Catal.* 2021, 11, 7477−7488

Read Online

ACCESS | Metrics & More | Article Recommendations | Supporting Information

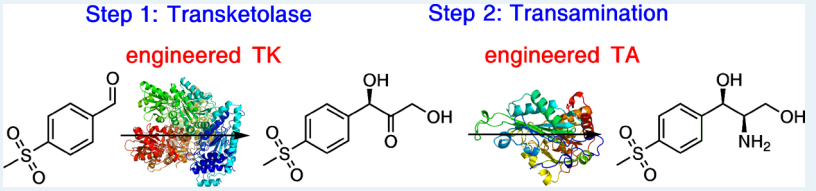

ABSTRACT: Florfenicol is the 3′-fluoro derivative of thiamphenicol and has been widely used in veterinary medicine for its high antibacterial activity and safety. However, the development of simplified and environmentally friendly catalytic methods for the stereoselective production of florfenicol is a key challenge. Herein, we established a highly stereoselective enzymatic one-pot reaction for the synthesis of an aminodiol intermediate of florfenicol bearing two stereocenters from industrial raw material 4-(methylsulfonyl) benzaldehyde by coupling transketolase (TK) and ω-transaminase (TA). The enantioselectivity of TK from *E. coli* was converted from (*S*) (93% ee) to (*R*) (95% ee), and we also inverted the enantiopreference ($E(S) = 9$ to $E(R) = 12$) and ketone/aldehyde substrate selectivity of TA ATA117 via structure-guided enzyme engineering. Docking calculations and molecular dynamics simulations of the wild-type and mutant enzymes unveiled the molecular basis for enzymatic stereocontrol. Using the engineered TK and TA, (1*R*,2*R*)-*p*-methylsulfonyl phenylserinol was biosynthesized with good yield (76%) and high stereoselectivity (96% de and >99% ee). Our work established an enzymatic synthetic route to (1*R*,2*R*)-*p*-methylsulfonyl phenylserinol, facilitating the development of a chemoenzymatic method for producing florfenicol.

KEYWORDS: *florfenicol, biocatalysis, TK, TA, stereoselectivity, one-pot reaction*

INTRODUCTION

Florfenicol [D-threo-3-fluoro-2-dichloroacetamido-1-(4-methylsulfonylphenyl)-1-propanol] is a synthetic, broad-spectrum fluorinated analogue of thiamphenicol (Figure 1A). Like chloramphenicol and thiamphenicol, it shows potent activity against many Gram-positive and Gram-negative bacteria.[1] Since adverse side effects, in particular dose-independent irreversible aplastic anemia, have been observed in animals, the EU legislation banned chloramphenicol from use in food-producing animals.[2] Meanwhile, the nitro group ($-NO_2$) in chloramphenicol is replaced by a methylsulfonyl group ($-SO_2CH_3$) in florfenicol; therefore, florfenicol would not cause dose-unrelated aplastic anemia. In addition, due to the replacement of the hydroxyl group at the C-3′ position with a fluorine in florfenicol, chloramphenicol-resistant strains, in which resistance is solely based on acetyltransferase activity, are susceptible to florfenicol. Multiple studies indicated that virtually all target bacteria isolated from respiratory tract infections of cattle and pigs are susceptible to florfenicol.[3−5] With its outstanding effectiveness and safety, florfenicol has been licensed exclusively for use in veterinary medicine. In the European Union, it has been approved for the treatment of respiratory tract infections in cattle in 1995 and in swine in 2000.[1,2]

Because of the large demand for florfenicol (4000 tons per year), there has been considerable attention on the development of different strategies for the synthesis of florfenicol[6−15] and the installation of the two adjacent stereocenters of *cis*-1,2-amino alcohols.[11,14] However, chemical approaches required multistep protection−deprotection, making the overall process cumbersome.[6,7,9,10,15] In addition, high toxicity of some chemical reagents and wastewater pollution raise other drawbacks in chemical synthesis. Moreover, some routes suffered from the use of transition-metal (e.g., Ru) complexes with chiral ligands that are toxic and difficult to obtain and remove.[15]

In view of the advantages of enzymatic catalysis, such as high regio-, chemo-, and stereoselectivity and without the require-

Received: March 17, 2021
Revised: May 28, 2021
Published: June 9, 2021

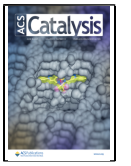

https://doi.org/10.1021/acscatal.1c01229
ACS Catal. 2021, 11, 7477−7488

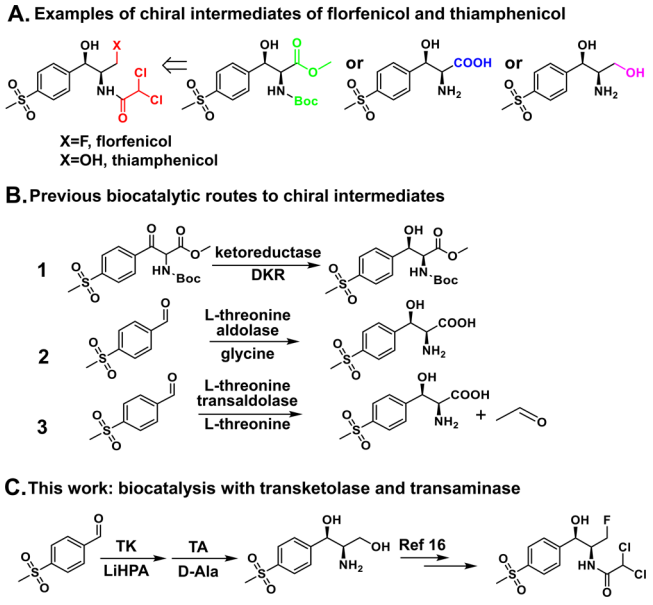

Figure 1. Synthesis of chiral intermediates of florfenicol and thiamphenicol. (A) Examples of chiral intermediates of florfenicol and thiamphenicol. (B) Previous synthetic methods using enzymes. (C) Our enzymatic route based on transketolase and transaminase. The aminodiol intermediate could be converted to the final florfenicol with fewer chemical steps than the reported intermediate.[16]

ment of protection and deprotection steps,[17−21] enzymatic catalysis could be a valuable alternative route for the chemical synthesis of the chiral florfenicol intermediate. A ketoreductase was reported to catalyze a stereoselective (2*S*,3*R*)-α-amino-β-hydroxyl ester formation from the corresponding α-amino-β-keto ester mediated by dynamic reductive kinetic resolution. In this approach, the majority of the product must be assembled in advance, with the enzyme mostly serving to set the stereochemistry at the end (Figure 1B, entry 1).[16] Besides, L-threonine aldolase (LTA) from *Pseudomonas putida* was reported to catalyze chiral L-threo-*p*-methylsulfonyl phenylserine (L-*threo*-MSPS) formation, whereas the diastereoselectivity of the reaction was relatively low, with 53% diastereomeric excess (de) (Figure 1B, entry 2).[22] The Zhu group performed enzyme engineering of an LTA from *Pseudomonas* sp. and obtained a mutant that catalyzed the formation of L-*threo*-MSPS with 71% de (Figure 1B, entry 2).[23] The Wu group also carried out enzyme engineering of an LTA from *Bacillus nealsonii* and obtained a mutant that catalyzed the formation of L-*threo*-MSPS with >99% de[24] (Figure 1B, entry 2). Recently, the Lin group reported an L-threonine transaldolase (LTTA) from *Pseudomonas* sp. Through conditional optimization, L-*threo*-MSPS was obtained with 94.6% de catalyzed by PsLTTA (Figure 1B, entry 3).[25,26] In general, L-*threo*-MSPS could be biosynthesized with good stereoselectivity using LTA or LTTA. To eventually be converted to florfenicol, L-*threo*-MSPS needs to be converted first to (1*R*,2*R*)-*p*-methylsulfonyl phenylserinol (**3a**), which requests two chemical steps comprising esterification and reduction.[27] In order to establish a simplified synthetic route of florfenicol, we attempted to achieve the biobased production of **3a**.

Recently, transketolases (TKs) have emerged as attractive biocatalysts for biotransformation of aliphatic and aromatic aldehydes to various chemicals.[28−36] TK is a thiamine pyrophosphate (ThDP)-dependent enzyme that catalyzes α-hydroxyketone formation by stereoselectively transferring a ketol unit from polyhydroxylated ketose phosphates as a "natural" donor to an aldehyde acceptor.[37] Several successful applications of TK have already been demonstrated for the production of α-hydroxyketones.[32−36] α-Hydroxyketones are of particular value as fine chemicals because of their utility as building blocks for the production of larger molecules, particularly for construction of heterocycles required in pharmaceuticals.[32] Akin to TKs, transaminases (TAs) have also attracted considerable interest in biocatalysis, both as an individual biocatalyst and as a part of multienzyme cascades for the synthesis of various amines.[38−42] TA catalyzes the transfer of an amino group between an amine donor (different amino acids and amines) and an amine acceptor (a ketone or aldehyde). Of particular interest are ω-TAs that do not require the presence of a carboxylic group in substrates, thereby accepting a large variety of carbonyl substrates.[38,39]

Here, we present an enzymatic one-pot two-step reaction for the synthesis of a stereoselective aminodiol intermediate, (1*R*,2*R*)-*p*-methylsulfonyl phenylserinol (**3a**), from readily available achiral 4-(methylsulfonyl)benzaldehyde (**1**) using a TK and a ω-TA (Figure 1C and Scheme 1). **1** is the raw material for the industrial production of florfenicol,[7] suggesting that our biocatalytic route has potential for industrial applications. However, there existed three challenges in this biocatalytic cascade reaction. First, TK family members are predominantly *S*-selective.[34] For aromatic aldehyde substrates, only one work reported an (*R*)-selective TK mutant that catalyzed the hydroxyketone formation toward benzaldehyde with 82% ee, but with a low conversion (10%).[36] Second, the hydroxyketone intermediate **2** formed by TK undergoes rapid racemization,[34] resulting in a decrease of optical purity. Third, **1** probably serves as a substrate for TK as well as for ω-TA, and ω-TA may display a higher chemical reactivity toward aldehyde **1** relative to ketone **2**.[43,44] As a consequence, most of **1** would be converted to the benzylamine side-product in the one-pot reaction. For addressing the first challenge, we reversed the enantioselectivity of TK from (*S*) (93% ee) to (*R*) (95% ee) via structure-guided enzyme engineering. For solving the second problem, we inverted the stereopreference of ω-TA toward chiral hydroxyketone intermediate **2** ($E(S)$ = 9 to $E(R)$ = 12). For addressing the third challenge, we reversed the aldehyde/ketone substrate selectivity of ω-TA. Combining the engineered TK and TA, the aminodiol intermediate (**3a**) of florfenicol was accessible with good yield (76%) and excellent stereoselectivity (96% de and >99% ee).

Scheme 1. One-Pot Two-Step Cascade Reaction to (1*R*,2*R*)-*p*-Methylsulfonyl Phenylserinol 3a, from the Industrial Raw Material 4-(Methylsulfonyl)-benzaldehyde 1

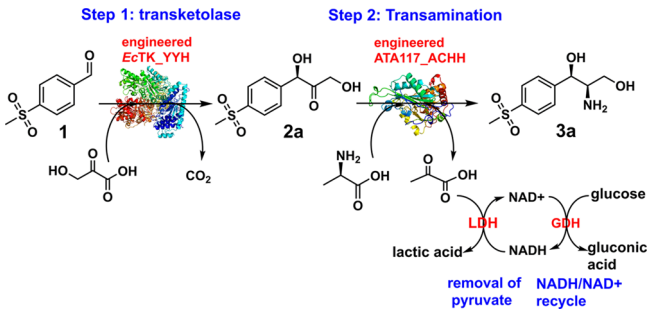

https://doi.org/10.1021/acscatal.1c01229
ACS Catal. 2021, 11, 7477−7488

RESULTS AND DISCUSSION

Choosing Suitable TKs and TAs for the Cascade Reaction. In the first step, β-hydroxypyruvate is decarboxylated and subsequently ligated to **1** yielding 1,3-dihydroxy-1-(4-(methylsulfonyl)phenyl)propan-2-one (**2**). The reaction is catalyzed by the ThDP-dependent TK. Initially, TKs for arylated aldehyde substrates were searched from the literature. Previous studies reported that the TK/D469T/R520Q/S385Y mutant from *E. coli* (*Ec*TK1) and TK/L382F/D470S mutant from *Geobacillus stearothermophilus* (*Gs*TK1) presented appealing biocatalytic activities for biotransformations involving nonpolar aromatic aldehyde.[34,35,45] On the other hand, the configuration of the hydroxyketone products indicated that *Gs*TK1 was (*S*)-stereoselective.[34] Therefore, *Ec*TK1 was tested using **1** as the substrate. As shown in Figure 2B, *Ec*TK1

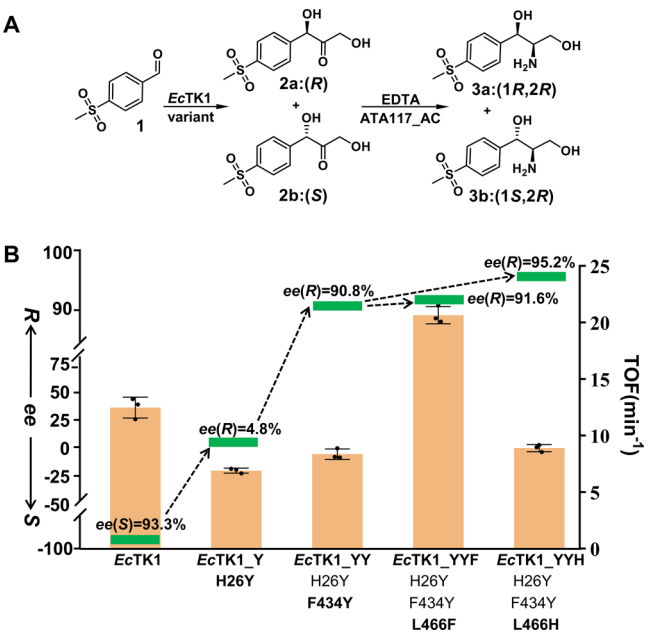

Figure 2. Enzyme engineering of *Ec*TK1 for enantioselective transketolase reaction. (A) Model reaction converting **1** to **2**. With combining ATA117_AC mutant enzyme, enantiomers **2a** and **2b** were converted to diastereomers **3a** and **3b**, respectively. The ee of **2** was thus determined by investigating the concentrations of **3a** and **3b**. (B) Enantioselectivities (green bar) and enzyme activities (orange bar) of the evolved variants of *Ec*TK1. Mutations in bold were added in the corresponding round of mutagenesis and screening. Dotted arrows denote a new round of site-specific mutagenesis.

catalyzed the conversion of **1** and β-hydroxypyruvate into **2** with acceptable activity (turnover frequency (TOF) ≥10/min). Using AutoDock 4.2, **1** was docked into the substrate binding site of the *Ec*TK1 crystal structure (PDB ID: 5hht).[35] ThDP was converted to the enamine-ThDP intermediate before docking according to the reaction mechanism of transketolase.[46] The docking analysis (Figure 3C) indicated that the R520Q mutation created a space for the methylsulfonyl moiety of **1**. T469 formed a hydrogen bond to the sulfonyl group, and H26 and H261 formed hydrogen bonds to the carbonyl group of **1**. We also observed that Y385 formed π−π stacking with the benzene ring of **1**. As a result of these mutations, **1** was properly oriented for catalysis (Figure 3C).[35]

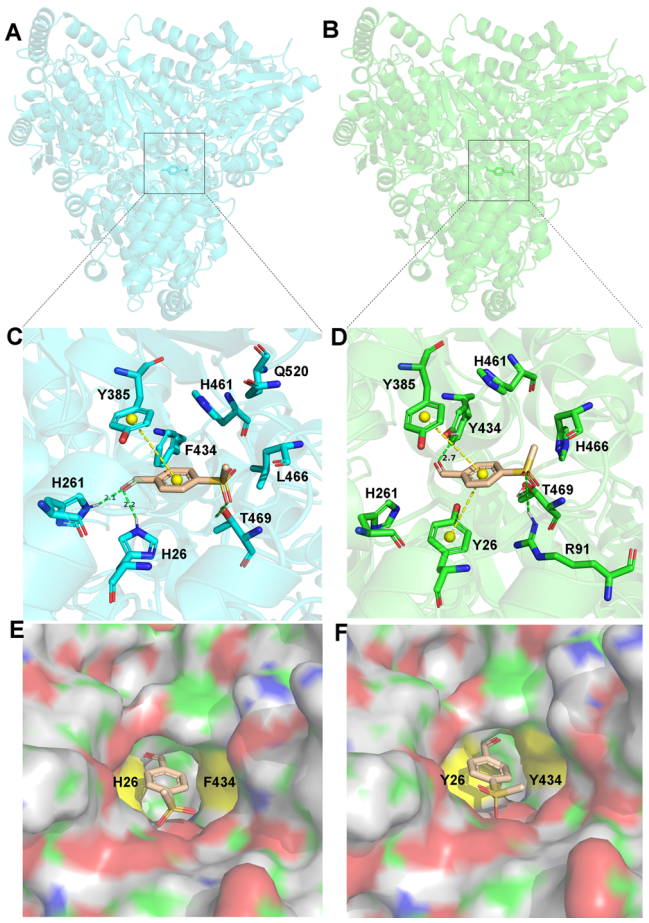

Figure 3. Molecular docking modes of aldehyde substrate **1** in *Ec*TK1 variants. Cartoon representation of **1** bound in (A) *Ec*TK1 (cyan) and (B) *Ec*TK1_YYH (green). (C) The enlarged binding mode of **1** in the *Ec*TK1 variant. **1** is shown in wheat. The key active pocket residues are shown in cyan. (D) The enlarged binding mode of **1** in the *Ec*TK1_YYH variant. **1** is shown in wheat. The key active pocket residues are shown in green. TPP is omitted for clarity. (E) The surface of the binding pocket of **1** bound to the *Ec*TK1 variant. (F) The surface of the binding pocket of **1** bound to the *Ec*TK1_YYH variant. **1** is shown in wheat. The key residues are represented by the yellow surface.

In the second step, **2** was transformed to final aminodiol product **3** catalyzed by the pyridoxal phosphate (PLP)-dependent ω-TA. Six different (*R*)-selective ω-TAs[47−50] were screened using **2** as the substrate, and ATA117 (a homolog of TA from *Arthrobacter* sp.) gave the most promising result (Figure S2). ATA117 is one of the most extensively used biocatalysts in both industrial and academic laboratories. It catalyzes the transamination of ketones with alanine or amines to produce chiral amines with the (*R*)-configuration.[48,51−56] The first and most prominent example was published by Merck & Co. and Codexis for the chiral synthesis of (*R*)-sitagliptin employing a protein-engineered variant of ATA117.[48]

Determining the Enantioselectivity of *Ec*TK1. After identifying potential catalyst candidates for the synthesis of **3a**, we attempted to determine the enantioselectivity of *Ec*TK1. In order to use achiral high-performance liquid chromatography (HPLC) to screen *Ec*TK1 mutants for their stereoselectivity, TK products (**2a** and **2b**) were converted into diastereomers **3a** and **3b** using a ω-TA without (or with very low) enantiopreference toward the chiral hydroxyketone **2**. There-

https://doi.org/10.1021/acscatal.1c01229
ACS Catal. 2021, 11, 7477−7488

fore, the enantiopreference of ATA117 was investigated using *racemic* **2** as the substrate. However, ATA117 was determined to display an obvious kinetic preference to the (*S*)-enantiomer with an *E* value of 8.5 (Figure 4, Figure S3, and Table S3). Therefore, we attempted to obtain ATA117 mutants that showed low kinetic selectivity toward **2** through enzyme engineering.

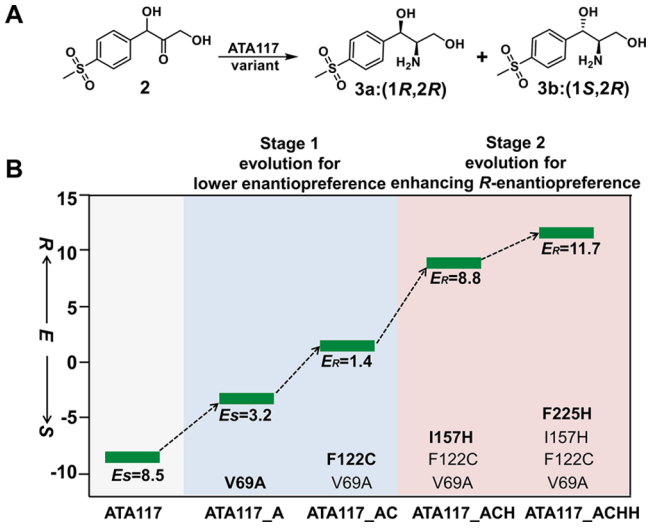

Figure 4. Enzyme engineering of the kinetic enantioselectivity of ATA117. (A) Model reaction converting *racemic* ketodiol **2** to aminodiol diastereomers **3a** and **3b**. (B) Cumulative improvement in the kinetic enantioselectivity of ATA117 resulting from the various iterative evolution steps of the present study. Mutations in bold were added in the corresponding round of mutagenesis and screening. Dotted arrows denote a new round of site-specific mutagenesis. $E = \ln[1 - C\times (1 + de)]/\ln[1 - C \times (1 - de)]$.[58,59]

A homology model of ATA117 was constructed using the structure of ω-TA from *Arthrobacter* sp. (PDB ID: 3wwh) as a guide. **2** was docked into its active site with the pyridoxamine-5′-phosphate (PMP) cofactor present using AutoDock 4.2. V69 and F122 located adjacent to the ligand **2** (Figure S4) in the small pocket were preferentially targeted for iterative site-saturation mutagenesis and screening since they were reported to be key sites for binding the substrate.[48] The variant ATA117/V69A/F122C (ATA117_AC) was obtained, which showed low kinetic enantioselectivity with an *E* value of 1.4 (Figure 4, Figure S3, and Table S3). Therefore, the ATA117/V69A/F122C (ATA117_AC) mutant enzyme was selected for determining the enantioselectivity of TK. In order to test the accuracy of the method for ee measurement using the ATA117_AC mutant, we designed and performed a pretest. The purified *rac*-**2** ($[\alpha]_D^{25} = 0$) was totally converted to almost equal amounts of **3a** and **3b** (**3a**/**3b** = 1:1.01) in 30 min at 25 °C using high loading (200 μM) of purified ATA117_AC (Figure S5B), which manifested that the ratio of **3a** and **3b** could accurately reflect the ratio of **2a** and **2b** using ATA117_AC under these conditions. To determine the enantioselectivity of TK, we performed transketolase reaction in a short time (20 min) at 25 °C owing to the tautomerization between **2a** and **2b** (Figure S5A,C,D)[34] while using high loading (100 μM) of purified *Ec*TK variant enzyme to ensure a high value of conversion (>80%). Subsequently, EDTA and purified ATA117_AC enzyme were added to the reaction mixture to quench the transketolase reaction by chelating Mg^{2+} and start the transamination in the same reaction conditions as the pretest. As shown in Figure 2 and Table S2, *Ec*TK1 displayed *S*-selectivity with 93.3% ee, which was in agreement with a previous study.[34]

Reversing the Enantioselectivity of *Ec*TK1 via Enzyme Engineering. Since *Ec*TK1 showed acceptable activity toward **1**, and its crystal structure (PDB ID: 5hht) has been reported,[35] we selected it as the starting template to reverse the enantioselectivity through structure-guided enzyme engineering. Using AutoDock 4.2, **1** was docked into the substrate binding site of *Ec*TK1. The most striking enzyme−substrate interactions in this model seemed to be the hydrogen bonds from H26 and H261 to the carbonyl group of **1** (Figure 3C). Residue F434 lined on the opposite side. We supposed that the orientation of the carbonyl group of **1** in the binding pocket would directly affect the stereoconfiguration of the hydroxyketone product. In order to reverse the stereoselectivity of TK, we devised a strategy dubbed "Break and Build", which is to break the existing hydrogen bonds from H26 and H261 to the carbonyl group of **1** first and then build a new one between the aldehyde carbonyl group and F434 on the opposite side via enzyme engineering. Therefore, H26 and H261 were first targeted for single site-saturation mutagenesis and screening. The enzyme libraries were expressed and screened as cell lysate catalysts in 24-well plates. To eliminate the influence of the tautomerization between (*R*)- and (*S*)-**2**, excess purified ATA117_AC enzyme was added to the reaction mixture to ensure the instantaneous conversion of hydroxyketone products, (*R*)- and (*S*)-**2**, into the corresponding (1*R*,2*R*)- and (1*S*,2*R*)-aminodiol diastereomers **3a** and **3b**, respectively. The site-saturation mutagenesis libraries of H26 and H261 were screened by HPLC. Among the mutants of the first generation, *Ec*TK1/H26Y (*Ec*TK1_Y) led to a reversion of enantioselectivity to (*R*)-**2a** (4.8% ee) (Figure 2 and Table S2). The switch in enantioselectivity may be attributed to the breakage of the existing hydrogen bonds from H26 to the carbonyl group of **1** because the introduction of a tyrosine with large steric hindrance at this position might alter the orientation of the carbonyl group of **1** in the active site. In order to build a new hydrogen bond between aldehyde carbonyl and F434, rational mutation of F434Y was introduced into *Ec*TK1_Y to yield the *Ec*TK1/H26Y/F434Y (*Ec*TK1_YY) mutant. As anticipated, *Ec*TK1_YY led to pronouncedly inverted stereoselectivity in favor of (*R*)-**2** with 90.8% ee (Figure 2 and Table S2). In order to further increase the enantioselectivity of TK, we attempted to find more targeted sites to be mutated. The docking results indicated that residues L466, H461, Y385, T469, and Q520 also lined in the binding pocket (Figure 3C). Among them, Y385, T469, and Q520 could not be mutated owing to their contribution in enzymatic activity toward **1**. Therefore, L466 and H461 were targeted for iterative site-saturation mutagenesis based on the *Ec*TK1_YY variant. Gratifyingly, the introduction of L466H (*Ec*TK1_YYH) and L466F (*Ec*TK1_YYF) exhibited increased (*R*)-enantioselectivity, with 95.2% ee and 91.6% ee, respectively (Figure 2 and Table S2). Based on mutant *Ec*TK1_YYH, H461 was subjected to site-saturation mutagenesis. However, no mutant was identified with enhanced (*R*)-selectivity. A homology model of *Ec*TK1_YYH was constructed, and **1** was docked into the substrate binding pocket. The docking analysis indicated that aldehyde carbonyl turned to the opposite side and formed a new hydrogen bond with the side chain of Y434.

https://doi.org/10.1021/acscatal.1c01229
ACS Catal. 2021, 11, 7477−7488

Additionally, the benzene ring of **1** formed $\pi-\pi$ stacking interactions with Y26 and Y385, and the sulfonyl group of **1** formed hydrogen bonds with T469 and R91. H466 might also form $\pi-\pi$ stacking interactions with Y434 since the aromatic rings of these two residues are coplanar (Figure 3D). These interactions together with the steric effect exerted by Y26 prompted the carbonyl group of **1** to adopt the inverted orientation (Figure 3D,F), which demonstrated the molecular basis of the switch in enantioselectivity from (*S*) to (*R*) of TK.

Since the poor solubility of **1** frustrated our ability to carry out Michaelis−Menten kinetics analysis, we could approximate the initial rate of hydroxyketone production under the reaction conditions by measuring the conversion at a short reaction time.[57] Figure 2B shows that the TOF of *Ec*TK1_YYH was lower than that of the parent *Ec*TK1 by 0.7-fold. The loss of enzyme activity might rise from the H26Y mutation. The introduction of tyrosine with large steric hindrance at this position might narrow down the binding pocket of the enzyme (Figure 3F), thus weakening the binding of the **1** substrate. Gratifyingly, the TOF of the *Ec*TK1_YYF variant was higher than that of *Ec*TK1 by 1.7-fold (Figure 2B).

Enhancing the (*R*)-Enantiopreference and Ketone/Aldehyde Substrate Selectivity of ATA117 via Enzyme Engineering. As the biocatalyst for the production of **2a** was achieved, we then turned to engineer ω-TA for the production of **3a** with high stereoselectivity. Therefore, we attempted to raise the (*R*)-enantiopreference of ATA117_AC via enzyme engineering. We constructed a homology model of ATA117_AC based on the crystal structure of ω-TA (PDB ID: 3wwh). The **2a** enantiomer was placed into the binding pocket to achieve a plausible nucleophilic attack for identifying steric clashes that could be alleviated by mutations. The docking model suggested that the side chain of I157 is positioned in proximity to the chiral hydroxyl of **2a** (2.5 Å), which is likely clashing with the chiral hydroxyl bound in the active site (Figure S6). So, I157 was chosen for saturation mutation based on the ATA117_AC variant. Except for enhancing the (*R*)-enantiopreference of TA, we attempted to concurrently promote the ketone/aldehyde substrate selectivity in order to reduce benzylamine side-product formation in the one-pot reaction. A challenge in this one-pot reaction is the fact that the starting material aldehyde serves as a substrate for TK as well as for the ω-TAs, and ω-TAs in principle possess higher chemical reactivity toward aldehydes than ketones.[43,44] Therefore, the site-saturation mutagenesis library of I157 was screened using 1 mM **1** and 2 mM *rac*-**2** (equal to the mix of 1 mM *S*-**2** and 1 mM *R*-**2**) as the substrates. ATA117_AC/I157H (ATA117_ACH) was identified, and its selectivity was re-examined using the purified enzyme. It is worth noting that the ATA117_ACH variant displayed dramatically increased (*R*)-enantiopreference with an *E* value of 8.8 (Figure 4, Figure S3, and Table S3), which outperformed the ATA117_AC by 6-fold. The enhancement in (*R*)-stereopreference induced by the I157H mutation could possibly be rationalized by the reduced steric hindrance and the formation of a new hydrogen bond between the histidine imidazolyl group and the hydroxyketone moiety of **2a** (Figure S7). Moreover, the ATA117_ACH variant showed reversed ketone/aldehyde substrate selectivity giving a 1.5:1 ratio of **3a**/(4-(methylsulfonyl)phenyl)-methanamine (MPMA, the amination product derived from **1**) compared to the 0.15:1 ratio observed for wild-type ATA117 (Figure S8). Thereafter, ATA117_ACH was used as the template for the next round of mutagenesis. Amino acid residues F225, W192, G224, A284, and T282 were targeted for iterative saturation mutation considering that these residues were close to the chiral hydroxyl group of **2a** in the docking complex (Figure S6). The introduction of F225H based on the ATA117_ACH variant (ATA117_ACHH) yielded increased (*R*)-enantiopreference with an *E* value of 11.7 (Figure 4, Figure S3, and Table S3) and improved ketone/aldehyde substrate selectivity (**3a**/MPMA = 1.9:1) (Figure S8). Using ATA117_ACHH as the template, the site-saturation mutation of W192, G224, A284, and T282 gave no promising result. In order to further investigate the kinetic enantiopreference of ATA117_ACHH, we performed kinetic resolution using 5 mM *rac*-**2** as the substrate. As shown in Figure S9, **3a** was yielded with good diastereoselectivity (81/19 diastereomer ratio) when the conversion reached 57% in 4 h.

To unveil the molecular basis leading to the (*R*)-enantiopreference of ATA117_ACHH, **2a** and **2b** were docked into the active site of the enzyme with the PMP cofactor present, respectively. The docked conformations of **2a** and **2b** in the active site were picked, where the keto group of the substrates faces the amino group of PMP allowing a nucleophilic attack to form to external aldimine. The resulting complexes (E:PMP + **2a** and E:PMP + **2b**) were energy-minimized and equilibrated to serve as starting conformations for MD simulations (Figure S10).[60,61] According to the mechanism of the transaminase-catalyzed reaction, the second half reaction was initiated by the nucleophilic attack on the bound substrate by the amino group of PMP.[60,61] Therefore, the distances between the cofactor PMP and the substrate ketone **2a** (d_{2a}) and **2b** (d_{2b}) were measured between the PMP's exocyclic nitrogen atom (PMP-NH_2) and the carbonyl carbon atom of the ketone (Figure 5B,C). Figure 5D and Figure S10D show that **2a** stayed in the active site throughout the 70 ns of simulation at a distance of ≈3.5 Å to PMP. This stood in stark contrast to the d_{2b}, which fluctuated markedly and ranged between 10 and 40 Å (Figure 5D and Figure S10D). These findings suggested that the marginal activity for **2b** seems to be relevant to the inability of the enzyme to initiate the catalytic cycle due to an unfavorable nucleophilic approach to the bound substrate. Furthermore, the elaborate analysis of the angular orientation of the bound substrate was performed, and the dihedral angle (θ_{DH}) between the plane harboring O_β, C_α, and N_{PMP} and the plane harboring O_β, C_α, and C_β was defined for the nucleophilic approach (Figure 5E).[60] The ideal θ_{DH} value for the nucleophilic attack on the carbonyl bond is known to be 90°.[62] The θ_{DH} in the complex of E:PMP + **2a** was concentratedly distributed and approached 75°, which allowed the unhindered and proximal nucleophilic attack. In contrast, θ_{DH} in the complex of E:PMP + **2b** was dispersed (Figure 5F). Therefore, both the distances of Cα-N_{PMP} and θ_{DH} endow the ATA117_ACHH variant with the (*R*)-enantiopreference.

One-Pot Cascade Reaction for 3a Synthesis. After obtaining the desired enzymes through engineering, the one-pot simultaneous cascade reaction for the synthesis of **3a** was first set up and optimized. Combining *Ec*TK_YYH and ATA117_ACHH, **3a** was biosynthesized with 40% yield, 93% de, and >99% ee (Table 1, entry 2). The loss in the yield mainly arose from the generation of the benzylamine by-product. Considering that the starting substrate aldehyde **1** is the substrate of TK and TA, TK with the high activity may increase the yield of the final product **3a**. Therefore, *Ec*TK_YYH was replaced by *Ec*TK_YYF that has much higher

https://doi.org/10.1021/acscatal.1c01229
ACS Catal. 2021, 11, 7477−7488

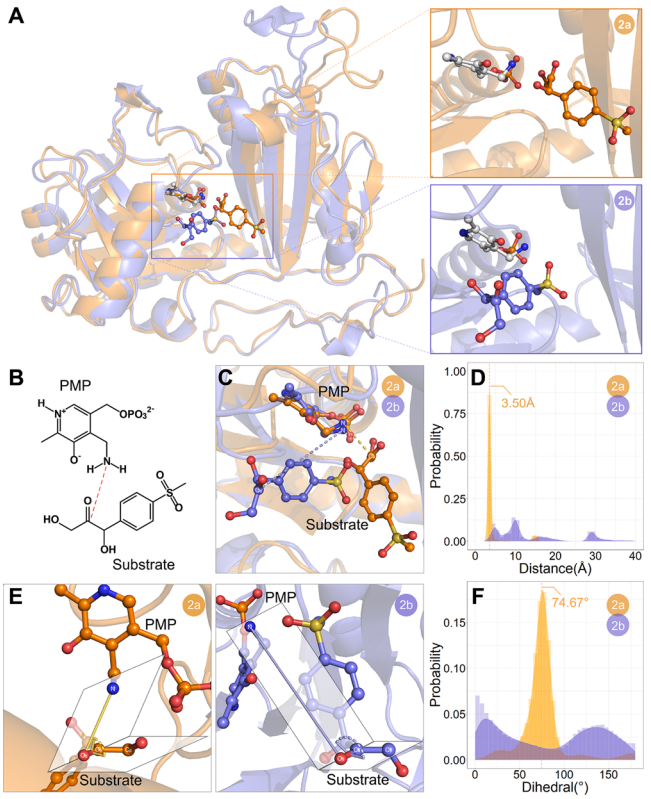

Figure 5. Statistics of molecular dynamics data. (A) Cartoon representation comparison of the **2a** enantiomer bound in ATA117_ACHH (orange) and **2b** enantiomer in ATA117_ACHH (blue). PMP is represented by the white stick. (B) Schematic diagram of the distance between the cofactor PMP and the substrate **2**. (C) Modeled complex for E:PMP + **2a**/**2b** after molecular dynamics (MD) simulation. The distances d_{2a} between the carbonyl carbon atoms of **2a** and the cofactor's amino group are marked as a yellow dotted line. The distances d_{2b} between the carbonyl carbon atoms of **2b** and the cofactor's amino group are marked as a blue dotted line. (D) Distribution of d_{2a} (yellow) and d_{2b} (blue) of all conformations in MD simulations. (E) Modeled complex for E:PMP + **2a**/**2b** after molecular dynamics (MD) simulation. The dihedral angle ($\theta_{DH\text{-}2a}$) between the plane harboring O_β, C_α, and N_{PMP} and the plane harboring O_β, C_α, and C_β of **2a** is marked as a yellow dotted line. The dihedral angle ($\theta_{DH\text{-}2b}$) between the plane harboring O_β, C_α, and N_{PMP} and the plane harboring O_β, C_α, and C_β of **2b** is marked as a blue dotted line. (F) Distribution of $\theta_{DH\text{-}2a}$ (yellow) and $\theta_{DH\text{-}2b}$ (blue) of all conformations in MD simulations.

activity (Figure 2B) in the reaction. Indeed, the yield and de have been improved (Table 1, entry 3).

To further reduce the formation of the benzylamine by-product and increase the yield and optical purity of **3a**, we performed one-pot cascade reaction in sequential mode without isolation and purification of the intermediate. First, 10 mM **1** was incubated with 60 μM purified *Ec*TK1_YYH for 1 h. Subsequently, 50 μM purified ATA117_ACHH was added to the reaction mixture and incubated for an extra 3 h. Additionally, NADH and LDH were used to drive the reversible equilibrium of transamination through removing the co-product pyruvic acid (Scheme 1). NADH can be regenerated using a well-established NADH-regenerating system, glucose/glucose dehydrogenase (Scheme 1).[40] An overall yield of 71% and a de value of 96% (Table 1, entry 7 and Figures S12, S13) were achieved at the optimized conditions. As a comparison, we also applied the *Ec*TK1_YYH and other ATA117 mutants to biosynthesize **3a**. The results showed that the ATA117 variant with higher (*R*)-enantiopreference would produce **3a** with a higher value of de (Table 1, entries 4−7). As expected, all products had a high enantiomeric purity of >99% (Table 1 and Figure S14).

We further developed a preparative scale (50 mL) of **3a** synthesis in one-pot two-step sequential cascade reaction. The pretest displayed better results (higher yield and optical purity of **3a**) using *Ec*TK_YYF with much higher activity instead of *Ec*TK_YYH, so *Ec*TK_YYF was chosen for the preparative scale. Applying 5 μmol of *Ec*TK1_YYF and 5 μmol of ATA117_ACHH, 92 mg (0.5 mmol) of **1** was converted to 93 mg of **3a** (0.38 mmol, 76% conversion) with a de value of 96% at 25 °C in 110 min, which corresponds to a space−time conversion of 24 g/L/day. After the reaction, the protein in the reaction mixture was precipitated using methanol. The resulting supernatant was concentrated and purified by reversed-phase chromatography with a PRC-ODS column (20 × 250 mm, pore size 15 μm) from SHIMADZU, and an 80 mg isolated product was obtained as a colorless oil, which corresponds to an isolated yield of 65% compared to the starting material. The product was confirmed by NMR (Figure S30).

One-Pot Cascade Reaction for (1*R*,2*R*)-Phenylserinol Derivative Synthesis. Encouraged by these results, we further investigated the substrate scope of the cascade reaction using various substituted benzaldehydes. The enzyme cascade combining *Ec*TK1_YYH and ATA117_ACHH in sequential mode for the synthesis of (1*R*,2*R*)-2-amino-1-(4-

Table 1. (1*R*,2*R*)-*p*-Methylsulfonyl Phenylserinol Produced by a Panel of Catalysts in One-Pot Cascade Reaction

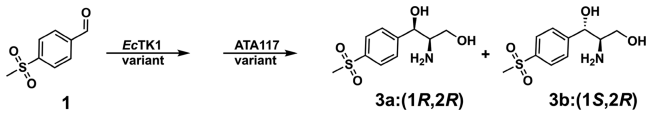

entry	one-pot reaction mode	catalyst	time (h)	yield[a] (%)	de (%)	ee (%)
1	simultaneous mode	*Ec*TK1_YYH + ATA117	4	24	43.1	>99
2		*Ec*TK1_YYH + ATA117_ACHH	4	40	93.0	>99
3		*Ec*TK1_YYF + ATA117_ACHH	4	51	94.4	>99
4	sequential mode	*Ec*TK1_YYH + ATA117	1 + 3	58	68.8	>99
5		*Ec*TK1_YYH + ATA117_AC	1 + 3	61	75.4	>99
6		*Ec*TK1_YYH + ATA117_ACH	1 + 3	73	92.1	>99
7		*Ec*TK1_YYH + ATA117_ACHH	1 + 3	71	96.0	>99

[a]Nonisolated yield [%] = ([product$_t$]/[substrate$_{t=0}$]) × 100; [product$_t$] was determined using the constructed calibration curves (Figure S11).

https://doi.org/10.1021/acscatal.1c01229
ACS Catal. 2021, 11, 7477−7488

Table 2. (1*R*,2*R*)-Phenylserinol Derivatives Produced by a Panel of Catalysts in Sequential One-Pot Cascade Reaction

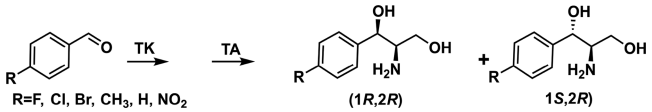

entry	R group	catalyst	yield (%)[a]	de (%)	ee (%)
1	F	*Ec*TK1_YYH + ATA117_ACHH	33	97.0	>99
2	F	*Ec*TK1_YYF + ATA117_ACHH	80	96.3	>99
3	Cl	*Ec*TK1_YYF + ATA117_ACHH	62	95.3	>99
4	Br	*Ec*TK1_YYF + ATA117_ACHH	72	94.7	>99
5	CH_3	*Ec*TK1_YYF + ATA117_ACHH	55	96.3	>99
6	H	*Ec*TK1_YYF + ATA117_ACHH	60	96.6	>99
7	NO_2	*Ec*TK1_YYF + ATA117_ACHH	51	94.5	>99

[a]Nonisolated yield [%] = ([product$_t$]/[substrate$_{t=0}$]) × 100; [product$_t$] were determined using the constructed calibration curves (Figure S11).

fluorophenyl)propane-1,3-diol ((1*R*,2*R*)-AFPPD) was first set up and optimized. The reaction gave moderate yield (33%) but very high stereoselectivity with 97% de and >99% ee (Table 2, entry 1). A potential bottleneck in the transformation of 4-(fluoro)benzaldehyde to AFPPD might be associated with the low activity of *Ec*TK1_YYH toward 4-(fluoro)benzaldehyde. Considering that *Ec*TK1_YYF showed 2−3-fold higher enzyme activity than *Ec*TK1_YYH, *Ec*TK1_YYF was thus combined to synthesize (1*R*,2*R*)-AFPPD. As expected, the cascade using *Ec*TK1_YYF gave a significantly increased yield (80%) and an equivalent stereoselectivity (96% de and >99% ee) (Table 2, entry 2 and Figures S15, S16, S22, S28). Moreover, other *para*-substituted benzaldehydes with both electron-donating and electron-withdrawing groups were well tolerated by the cascade reaction combining *Ec*TK1_YYF and ATA117_ACHH, enabling the highly diastereo- and enantioselective (95−97% de and >99% ee) synthesis of the corresponding aminodiol products with moderate to good yields (51−72%) within 6 h (Table 2, entries 3−7 and Figures S15 and S17−S28). Notably, the *para*-substituted phenylserinols with fluorine, chlorine, and bromine groups furnished in our cascade reaction possessed higher conversion and higher de values than the reported corresponding *para*-substituted intermediates of florfenicol,[24,26,63] which suggested that our cascade route exhibited a broad substrate scope.

Although benzaldehyde derivatives bear different *para*-substitutions, they gave all products with absolute enantioselectivity (>99% ee) (Tables 1 and 2), which suggested that the evolved mutations (V69A/F122C/I157H/F225H) of ATA117 responsible for manipulating the enantiopreference toward the chiral hydroxyketone do not impair the innate (*R*)-stereospecificity of the enzyme. For the D-amino acid aminotransferase (Fold Type IV) to which ATA117 belongs, the active site lysine (e.g., lys188 in ATA117) is positioned on the *re* face of the quinonoid intermediate and the *si* face is solvent-exposed, and therefore, the nucleophilic attack by amino donor PMP occurs at the *re* face of the substrate to exclusively give the (*R*)-configuration.[64]

CONCLUSIONS

In summary, in order to achieve the biosynthesis of the chiral aminodiol intermediate of florfenicol, (1*R*,2*R*)-*p*-methylsulfonyl phenylserinol **3a**, multiple rounds of structure-guided iterative site-saturation mutagenesis of TK and TA were conducted to reverse the enzymatic stereoselectivity. This study firstly obtained a highly (*R*)-selective TK enzyme toward aromatic aldehyde through three rounds of site-saturation mutagenesis and rational mutation. Moreover, the kinetic enantiopreference of TA was also successfully inverted via four rounds of site-saturation mutagenesis. The evolved ATA117_ACHH mutant showed higher activity toward ketone relative to the aldehyde substrate, which is a rare event for ω-TA. Combining the engineered *Ec*TK1_YYH or *Ec*TK1_YYF and ATA117_ACHH, **3a** was accessible with 71−76% yield and 96% de in sequential one-pot cascade reaction. Overall, our study established an efficient biocatalytic route to **3a**, a chiral intermediate of florfenicol, which required fewer subsequent steps to produce florfenicol than the reported intermediates.

EXPERIMENTAL SECTION

General Methods and Materials. The (1*R*,2*R*)-*p*-methylsulfonyl phenylserinol (**3a**) standard was bought from Huangshi Yongxin Biotechnology Co. (Huangshi, Hubei, China). (1*S*,2*S*)-2-Amino-1-phenylpropane-1,3-diol and (1*S*,2*S*)-2-amino-1-(4-nitrophenyl)propane-1,3-diol were bought from Sigma-Aldrich Co. (Shanghai, China). (1*R*,2*R*)-2-Amino-1-phenylpropane-1,3-diol was bought from Jiangsu Aikang Biomedicine Co. (Nanjing, Jiangsu, China). (1*R*,2*R*)-2-Amino-1-(4-nitrophenyl)propane-1,3-diol was bought from TCI Co. (Shanghai, China). (1*R*,2*R*)-2-Amino-1-(4-bromophenyl)propane-1,3-diol was bought from Nanjing Zhicui Biotechnology Co. (Nanjing, Jiangsu, China). (*Erythro*)- and (*threo*)-2-amino-1-(4-fluorophenyl)propane-1,3-diol, (*erythro*)- and (*threo*)-2-amino-1-(4-chlorophenyl)propane-1,3-diol, and (*erythro*)- and (*threo*)-2-amino-1-(*p*-tolyl)-propane-1,3-diol were bought from Shanghai Kaishu Chemical Technology Co. (Shanghai, China). Lithium hydroxypyruvate (LiHPA) was purchased from Sigma-Aldrich Co. (Shanghai, China). Thiamine diphosphate (ThDP), pyridoxal-5′-phosphate hydrate (PLP), glucose, and glucose dehydrogenase (GDH) were purchased from Aladdin Co. (Shanghai, China). The reduced form of nicotinamide-adenine dinucleotide (NADH) and D-Ala were purchased from TCI Co. (Shanghai, China). Lactate dehydrogenase (LDH) was purchased from Sinopharm (Shanghai, China). The materials used for culture media, including peptone, yeast extract, and agar, were purchased from OXOID (Shanghai, China). The Phanta Max Super-Fidelity DNA Polymerase was obtained from Vazyme Co. (Shanghai, China). The restriction enzyme Dpn I was bought from Thermo Scientific (Shanghai, China). The oligonucleotides were synthesized, and DNA sequencing was conducted by Shanghai BioSune (Shanghai, China). The PCR extraction kit and the plasmid mini kit used for extracting

https://doi.org/10.1021/acscatal.1c01229
ACS Catal. 2021, 11, 7477−7488

plasmids were bought from Vazyme Co. (Shanghai, China). The lysogeny broth (LB) medium contained 10 g/L tryptone, 5 g/L yeast extract, and 10 g/L NaCl. The *racemic* 1,3-dihydroxy-1-(4-(methylsulfonyl)-phenyl)-propan-2-one was prepared by the transketolase reaction of 4-(methylsulfonyl)-benzaldehyde with hydroxypyruvate catalyzed by *Ec*TK1. The NMR spectra were measured on a Bruker Avance 600 using MeOD as the solvent.

Molecular Docking. The substrates **2** and **2a** were docked into the binding pocket of ATA117 and the homology model of ATA117 mutants (ATA117_AC and ATA117_ACH), respectively, using the position of PLP in the bound ligand of 3wwh as a guide with AutoDock 4.2. The catalytic lysine (K188) was deprotonated, and the PLP was converted to PMP before docking. Postdocking, the conformations obtained were filtered to derive a plausible attack conformation.[61]

The substrate **1** was docked into the binding pocket of the *Ec*TK1 structure (PDB ID: 5hht) and the homology model of *Ec*TK1_YYH. The *Ec*TK1 structure was stripped of all crystallographic waters. ThDP was converted to the enamine-ThDP intermediate before docking. The explorable space for docking was defined as a cube 15 Å in length centered at 23.489, 15.398, and 5.953 including the entire active-site and omitting the surface hydrophobic pockets.[35] Resulting poses were analyzed and checked for hydrogen bonding in the PyMOL Molecular Graphics System. Only the most energetically favorable pose-clusters were retained. Among them, poses that were observed to be potentially "catalytically productive" were selected. Catalytically productive was taken to mean orientations of the benzene ring that point the reactive aldehyde group close to the enamine-ThDP intermediate.[35]

MD Simulations. The ligands **2a** and **2b** were docked into the homology model of the ATA117_ACHH mutant using AutoDock 4.2. First, optimization was accomplished using the Gaussian09 program at the level of b3lyp/6-31 g(d) followed by calculation of the electrostatic surface potential (ESP) charge. Subsequently, restrained electrostatic potential (RESP) charge fitting was applied using the Multiwfn program. The parameter preparation for PMP and the substrate molecules **2a** and **2b** was performed by using the Antechamber package. Finally, the GPU version of the PMEMD[65] engine integrated with the Amber 16 package and FF14SB force field[66] was used for the MD simulations. The enzyme−ligand complex was placed in a solvent box of the TIP3P water model with a shell of 10 Å thick.

The entire systems were first subjected to energy minimization using the 5000-step steepest descent followed by the conjugate gradient algorithm for 5000 steps. The system was then subjected to 1400 ps controlled heating using a Langevin thermostat with a collision frequency of 10 ps^{-1}, which requires the temperature to be increased from 0 to 300 K during the first 1000 ps. The protein and the ligand molecules were heated with a harmonic potential restraint of 5 $kcal{\cdot}mol^{-1}{\cdot}Å^2$. The system was then equilibrated at 300 K using the NPT ensemble for 200 ps to facilitate adjustment of the system to the appropriate density and dimension. Finally, the molecular dynamics simulations were performed without any restraint under NPT conditions at 300 K for 100 ns with a step time of 2 fs. The Berendsen barostat[67] was used to maintain the pressure at 1 bar during the equilibration and production MD phase. The SHAKE algorithm was used to constrain the lengths of all the bonds involving hydrogen atoms during the whole procedure. The long-range electrostatic interactions were calculated using the Particle Mesh Ewald (PME) method.[68] The CPPTRAJ[69] tool implemented in AMBER was used to conduct the structural analyses of the molecular dynamics trajectory, such as the distance and dihedral of atoms in the ligand molecule, root-mean-square deviation (RMSD), and cluster analysis. The structure figures were prepared using PyMOL.

Construction of TK and TA Mutant Libraries. Plasmid pET28a (Novagen) was used as a cloning and expression vector for TK variants, and plasmid pRSFduet (Novagen) was used as a cloning and expression vector for TA variants described in this paper. The saturation mutagenesis libraries of H26, L466, V69, F122, I157, F225, and etc. were generated utilizing degenerate oligos (i.e., NNK) to incorporate mutations at the targeted position. On the basis of the *Ec*TK1 and ATA117 or related mutant sequence, appropriate primers were designed. The mutant genes were then constructed by using PCR amplification methods with a Phanta Max Super-Fidelity DNA Polymerase. The PCR products were analyzed on agarose gel by electrophoresis. The PCR products were digested with the Dpn I restriction enzyme at 37 °C for more than 4 h to remove the template DNA. After digestion, the products were directly transformed to commercial *E. coli* BL21 (DE3) by heat shock. Diluted transformation mixtures (about 1/7) were spread on agar plates containing 50 μg/mL kanamycin and grown overnight at 37 °C. The individual clones with the expected mutation evaluated by DNA sequencing were picked.

Screening of TK and AT Mutant Libraries. *E. coli* BL21 (DE3) cells carrying the recombinant plasmid were cultivated in 1 mL of LB medium containing kanamycin (50 μg/mL) using a 24 shallow-well plate at 37 °C and 220 rpm for 12 h. 40 μL of the overnight culture was transferred to a 24 deep-well plate with a fresh lysogeny broth medium (4 mL/well) and was cultivated under the same conditions. When the OD_{600} reached 0.6−0.8, isopropyl β-D-thiogalactoside (IPTG) was added to a final concentration of 0.15 mM. After continuing cultivation at 20 °C for 18 h, the cell pellets were harvested and washed with 1 mL of Tris−HCl Buffer (50 mM, 150 mM NaCl, pH 7.5) and centrifuged for 20 min with 4000 rpm at 4 °C. The precipitate was frozen at −80 °C and thawed once. The cells were resuspended in 250 μL of the same buffer and lysed by ultrasonication (2 s on and 4 s off; 30 cycles). Cell debris was removed by centrifugation at 4 °C.

For screening of TK mutant libraries, purified ATA117_AC enzyme, which showed low kinetic selectivity toward the chiral hydroxyketone, was combined to ensure the instantaneous conversion of hydroxyketone intermediate, which was apt to undergo racemization.[34] By combining ATA117_AC, (*S*)- and (*R*)-hydroxyketone were converted to the corresponding (1*R*,2*R*)- and (1*S*,2*R*)-aminodiol diastereomers **3a** and **3b**, respectively. The 100 μL screening system contained 40 μL of supernatant, 50 mM Tris−HCl buffer, 5 mM **1** substrate, 5 equiv of LiHPA, 2.4 mM ThDP, 9 mM $MgCl_2$, 1 mM PLP, 200 mM D-Ala, 5 equiv of NADH, 45 U/mL LDH, and 20 μM purified ATA117_AC variant enzyme. Aminodiol diastereomer products were measured by HPLC using a Super-C18 column.

For screening of TA mutant libraries, equivalent **2a**, **2b**, and **1** were used as the substrates in order to concurrently promote the (*R*)-enantiopreference and ketone/aldehyde substrate selectivity of TA. Therefore, the 100 μL screening system contained 40 μL of supernatant, 50 mM Tris−HCl buffer, 2 mM *rac*-**2**, 1 mM **1**, 200 mM D-Ala, and 1 mM PLP. Aminodiol

https://doi.org/10.1021/acscatal.1c01229
ACS Catal. 2021, 11, 7477−7488

and benzylamine products were measured by HPLC using a Super-C18 column.

Measurement of Enantioselectivity for *Ec*TK1 Mutant Enzymes. The 100 μL reaction system contained 50 mM Tris−HCl buffer (pH 7), 5 mM **1**, 25 mM LiHPA, 9 mM $MgCl_2$, and 4.8 mM ThDP. The reaction was initiated by addition of 100 μM TK enzyme. After reacting 20 min at 25 °C, the reaction was quenched by addition of 18 mM EDTA for chelating Mg^{2+} that was indispensable for TK activity. Subsequently, 20 μL of reaction mixture was added to a new 100 μL reaction system that contained 200 mM D-Ala, 2 mM PLP, 20 mM NADH, 90 U/mL LDH, and 200 μM purified ATA117_AC enzyme. Thus, chiral hydroxyketone enantiomers yielded at the first step were fully converted to aminodiol diastereomers **3a** and **3b** in 30 min at 25 °C. The aminodiol products **3a** and **3b** were measured by HPLC using a Super-C18 column.

Measurement of *E* for the ATA117 Mutant Enzyme. The *E* values of the purified ATA117 variants toward the transamination of *rac*-**2** were determined referring to previous research.[58,59] *E* was measured in a 100 μL reaction system that contained 50 mM Tris−HCl buffer (pH 7.5), 2 mM *rac*-**2**, 200 mM D-Ala, 2 mM PLP, and 5−40 μM ATA117 variants depending on the activity. The concentrations of purified enzymes ATA117, ATA117_A, ATA117_AC, ATA117_ACH, and ATA117_ACHH were set to be 5, 20, 20, 40, and 40 μM, respectively. After reacting for 1 h at 30 °C, the reaction was quenched by addition of 200 μL of methanol. Samples were measured by HPLC using a Super-C18 column.

Simultaneous One-Pot Cascade Reaction to (1*R*,2*R*)-*p*-Methylsulfonyl Phenylserinol 3a. The 100 μL reaction system employing *Ec*TK1_YYH and ATA117_ACHH (or ATA117) contained 50 mM HEPES buffer (pH 8), 5 mM **1**, 25 mM LiHPA, 18 mM $MgCl_2$, 4.8 mM ThDP, 60 μM purified enzyme *Ec*TK1_YYH, 50 mM D-Ala, 2 mM PLP, 3 equiv of NADH, 90 U/mL LDH, and 30 μM purified enzyme ATA117_ACHH (or ATA117). The reaction mixture was incubated at 25 °C for 4 h.

The 100 μL reaction system employing *Ec*TK1_YYF and ATA117_ACHH contained 50 mM HEPES buffer (pH 8), 5 mM **1**, 25 mM LiHPA, 18 mM $MgCl_2$, 4.8 mM ThDP, 60 μM purified enzyme *Ec*TK1_YYF, 50 mM D-Ala, 2 mM PLP, 3 equiv of NADH, 45 U/mL LDH, and 40 μM purified enzyme ATA117_ACHH. The reaction mixture was incubated at 25 °C for 4 h.

Sequential One-Pot Cascade Reaction to (1*R*,2*R*)-*p*-Methylsulfonyl Phenylserinol 3a. The 100 μL reaction system contained 100 mM Tris−HCl buffer (pH 7.5), 5 mM **1**, 15 mM LiHPA, 18 mM $MgCl_2$, 4.8 mM ThDP, 30 μM purified enzyme *Ec*TK1_YYH, 200 mM D-Ala, 2 mM PLP, 200 mM glucose, 2 equiv of NADH, 90 U/mL LDH, 30 U/mL GDH, and 50 μM purified enzyme ATA117 variants. For the first transketolase reaction step, **1**, LiHPA, Tris−HCl, $MgCl_2$, ThDP, and *Ec*TK1_YYH were added into the reaction vessel and incubated at 25 °C for 1 h. For the second transamination step, D-Ala, PLP, glucose, NADH, LDH, GDH, and ATA117 variants were added to the reaction mixture and incubated at 25 °C for an additional 1−4 h.

Preparative Scale of (1*R*,2*R*)-*p*-Methylsulfonyl Phenylserinol 3a Synthesis. A preparative scale (50 mL) of the one-pot two-step cascade to **3a** has been developed. In the first step, 16.7 mM **1** was converted with 3 equiv of LiHPA and 167 μM purified *Ec*TK1_YYF in a 30 mL reaction system for 35 min at 25 °C. **1** was added in 5.6 mM batches every 10 min considering the insolubility of the aldehyde substrate. The second step was initiated by adding 20 mL of transamination reaction mixture. The total 50 mL reaction system contained 100 μM purified ATA117_ACHH enzyme, 200 mM D-Ala, 2 equiv of NADH, 90 U/mL LDH, 200 mM glucose, and 30 U/mL GDH. The reaction mixture was incubated at 25 °C for an additional 75 min.

Sequential One-Pot Cascade Reaction to (1*R*,2*R*)-Phenylserinol Derivatives. For (1*R*,2*R*)-*p*-fluorine phenylserinol, *p*-chlorine phenylserinol, *p*-methyl phenylserinol, and phenylserinol biosynthesis, the 100 μL reaction system contained 100 mM Tris−HCl buffer (pH 7.5), 5 mM benzaldehyde derivatives, 15 mM LiHPA, 18 mM $MgCl_2$, 4.8 mM ThDP, 50 μM purified enzyme *Ec*TK1_YYF, 200 mM D-Ala, 2 mM PLP, 200 mM glucose, 2 equiv of NADH, 90 U/mL LDH, 30 U/mL GDH, and 50 μM purified enzyme ATA117_ACHH. For the first transketolase reaction step, **1**, LiHPA, $MgCl_2$, ThDP, and *Ec*TK1_YYF were added into the reaction vessel and incubated at 25 °C for 1.0, 1.5, 2.0, 2.5, and 3.0 h. For the second transamination step, D-Ala, PLP, glucose, NADH, LDH, GDH, and ATA117_ACHH were added to the reaction mixture and incubated at 25 °C for an additional 3 h.

For (1*R*,2*R*)-*p*-bromine phenylserinol biosynthesis, the 100 μL reaction system contained 100 mM Tris−HCl buffer (pH 7.5), 6% DMSO, 5 mM 4-bromobenzaldehyde, 15 mM LiHPA, 18 mM $MgCl_2$, 4.8 mM ThDP, 50 μM purified enzyme *Ec*TK1_YYF, 200 mM D-Ala, 2 mM PLP, 200 mM glucose, 2 equiv of NADH, 90 U/mL LDH, 30 U/mL GDH, and 50 μM purified enzyme ATA117_ACHH. For the first transketolase reaction step, 4-bromobenzaldehyde, LiHPA, $MgCl_2$, ThDP, and *Ec*TK1_YYF were added into the reaction vessel and incubated at 25 °C. Among them, the 4-bromobenzaldehyde substrate was added in two batches. The second half of the 4-bromobenzaldehyde substrate was added after 1 h. The reaction mixture was then incubated for 1.0, 1.5, and 2.0 h. For the second transamination step, D-Ala, PLP, glucose, NADH, LDH, GDH, and ATA117_ACHH were added to the reaction mixture and incubated at 25 °C for an additional 3 h.

For (1*R*,2*R*)-*p*-nitro phenylserinol biosynthesis, the 100 μL reaction system contained 100 mM Tris−HCl buffer (pH 7.5), 5% DMSO, 5 mM 4-nitrobenzaldehyde, 20 mM LiHPA, 18 mM $MgCl_2$, 4.8 mM ThDP, 60 μM purified enzyme *Ec*TK1_YYF, 200 mM D-Ala, 2 mM PLP, 200 mM glucose, 2 equiv of NADH, 90 U/mL LDH, 30 U/mL GDH, and 60 μM purified enzyme ATA117_ACHH. For the first transketolase reaction step, 4-nitrobenzaldehyde, LiHPA, $MgCl_2$, ThDP, and *Ec*TK1_YYF were added into the reaction vessel and incubated at 25 °C for 2.7 h. For the second transamination step, D-Ala, PLP, glucose, NADH, LDH, GDH, and ATA117_ACHH were added to the reaction mixture and incubated at 25 °C for an extra 2, 3, 4, and 5 h.

■ ASSOCIATED CONTENT

Supporting Information

The Supporting Information is available free of charge at https://pubs.acs.org/doi/10.1021/acscatal.1c01229.

Experimental section, primers used for site-directed saturated mutagenesis, transketolase reaction data presented in Figure 2 of the main text, enantioselective transamination of *rac*-**2** with ATA117 variants, HPLC

https://doi.org/10.1021/acscatal.1c01229
ACS Catal. 2021, 11, 7477−7488

analytical methods of aminodiol derivatives, HPLC analytical methods for ee measurement of aminodiol derivatives, LC−MS, screening, HPLC, molecular docking results, time course data, kinetic resolution data, mass data, NMR data, and sequence information (PDF)

AUTHOR INFORMATION

Corresponding Author

Shuangjun Lin − *Frontiers Science Center for Transformative Molecules, Shanghai Jiao Tong University, Shanghai 200240, China; State Key Laboratory of Microbial Metabolism, Joint International Research Laboratory on Metabolic & Developmental Sciences, School of Life Sciences & Biotechnology, Shanghai Jiao Tong University, Shanghai 200240, China;* orcid.org/0000-0001-9406-9233; Email: linsj@sjtu.edu.cn

Authors

Qi Liu − *State Key Laboratory of Microbial Metabolism, Joint International Research Laboratory on Metabolic & Developmental Sciences, School of Life Sciences & Biotechnology, Shanghai Jiao Tong University, Shanghai 200240, China*

Xinyue Xie − *State Key Laboratory of Microbial Metabolism, Joint International Research Laboratory on Metabolic & Developmental Sciences, School of Life Sciences & Biotechnology, Shanghai Jiao Tong University, Shanghai 200240, China*

Mancheng Tang − *State Key Laboratory of Microbial Metabolism, Joint International Research Laboratory on Metabolic & Developmental Sciences, School of Life Sciences & Biotechnology, Shanghai Jiao Tong University, Shanghai 200240, China;* orcid.org/0000-0001-9418-3239

Wentao Tao − *State Key Laboratory of Microbial Metabolism, Joint International Research Laboratory on Metabolic & Developmental Sciences, School of Life Sciences & Biotechnology, Shanghai Jiao Tong University, Shanghai 200240, China*

Ting Shi − *State Key Laboratory of Microbial Metabolism, Joint International Research Laboratory on Metabolic & Developmental Sciences, School of Life Sciences & Biotechnology, Shanghai Jiao Tong University, Shanghai 200240, China;* orcid.org/0000-0003-3921-4412

Yuanzhen Zhang − *State Key Laboratory of Microbial Metabolism, Joint International Research Laboratory on Metabolic & Developmental Sciences, School of Life Sciences & Biotechnology, Shanghai Jiao Tong University, Shanghai 200240, China*

Tingting Huang − *State Key Laboratory of Microbial Metabolism, Joint International Research Laboratory on Metabolic & Developmental Sciences, School of Life Sciences & Biotechnology, Shanghai Jiao Tong University, Shanghai 200240, China*

Yilei Zhao − *State Key Laboratory of Microbial Metabolism, Joint International Research Laboratory on Metabolic & Developmental Sciences, School of Life Sciences & Biotechnology, Shanghai Jiao Tong University, Shanghai 200240, China;* orcid.org/0000-0003-4687-7847

Zixin Deng − *State Key Laboratory of Microbial Metabolism, Joint International Research Laboratory on Metabolic & Developmental Sciences, School of Life Sciences & Biotechnology, Shanghai Jiao Tong University, Shanghai 200240, China*

Complete contact information is available at: https://pubs.acs.org/10.1021/acscatal.1c01229

Notes

The authors declare no competing financial interest.

ACKNOWLEDGMENTS

We thank Mrs. J. Wu at the Instrumental Analysis Center of SJTU for performing the NMR experiments. This work was financially supported by the National Key Research and Development Program of China (grant no. 2018YFA0901900) and the National Science Foundation of China (21632007 and 31425001).

REFERENCES

(1) Kehrenberg, C.; Schwarz, S. Distribution of Florfenicol Resistance Genes fexA and cfr among Chloramphenicol-Resistant Staphylococcus Isolates. *Antimicrob. Agents Chemother.* **2006**, *50*, 1156−1163.

(2) Schwarz, S.; Kehrenberg, C.; Doublet, B.; Cloeckaert, A. Molecular basis of bacterial resistance to chloramphenicol and florfenicol. *FEMS Microbiol. Rev.* **2004**, *28*, 519−542.

(3) Kehrenberg, C.; Mumme, J.; Wallmann, R.; Verspohl, J.; Tegeler, R.; Kühn, T.; Schwarz, S. Monitoring of florfenicol susceptibility among bovine and porcine respiratory tract pathogens collected in Germany during the years 2002 and 2003. *J. Antimicrob. Chemother.* **2004**, *54*, 572−574.

(4) Schwarz, S.; Kehrenberg, C.; Salmon, S. A.; Watts, J. L. In vitro activities of spectinomycin and comparator agents against Pasteurella multocida and Mannheimia haemolytica from respiratory tract infections of cattle. *J. Antimicrob. Chemother.* **2004**, *53*, 379−382.

(5) Priebe, S.; Schwarz, S. In vitro activities of florfenicol against bovine and porcine respiratory tract pathogens. *Antimicrob. Agents Chemother.* **2003**, *47*, 2703−2705.

(6) Schumacher, D. P.; Clark, J. E.; Murphy, B. L.; Fischer, P. A. An Efficient Synthesis of Florfenicol. *J. Org. Chem.* **1990**, *55*, 5291−5294.

(7) Wu, G.; Schumacher, D. P.; Tormos, W.; Clark, J. E.; Murphy, B. L. An Improved Industrial Synthesis of Florfenicol plus an Enantioselective Total Synthesis of Thiamphenicol and Florfenicol. *J. Org. Chem.* **1997**, *62*, 2996−2998.

(8) Bhaskar, G.; Satish Kumar, V.; Venkateswara Rao, B. A short stereoselective synthesis of (−)-chloramphenicol and (+)-thiamphenicol. *Tetrahedron: Asymmetry* **2004**, *15*, 1279−1283.

(9) George, S.; Narina, S. V.; Sudalai, A. A short enantioselective synthesis of (−)-chloramphenicol and (+)-thiamphenicol using tethered aminohydroxylation. *Tetrahedron* **2006**, *62*, 10202−10207.

(10) Lu, W.; Chen, P.; Lin, G. New stereoselective synthesis of thiamphenicol and florfenicol from enantiomerically pure cyanohydrin: a chemo-enzymatic approach. *Tetrahedron* **2008**, *64*, 7822−7827.

(11) Li, F.; Wang, Z.-H.; Zhao, L.; Chen, F.-E. A Facile and Efficient Asymmetric Synthesis of Florfenicol. *Synlett* **2011**, *2011*, 2883−2885.

(12) Li, F.; Wang, Z.-H.; Zhao, L.; Xiong, F.-J.; He, Q.-Q.; Chen, F.-E. An efficient enantioselective synthesis of florfenicol via a vanadium-catalyzed asymmetric epoxidation. *Tetrahedron: Asymmetry* **2011**, *22*, 1337−1341.

(13) Wang, Z.; Li, F.; Zhao, L.; He, Q.; Chen, F.; Zheng, C. An efficient enantioselective synthesis of florfenicol via asymmetric aziridination. *Tetrahedron* **2011**, *67*, 9199−9203.

(14) Wang, Z.-H.; Zheng, C.; Li, F.; Zhao, L.; Chen, F.-E.; He, Q.-Q. An Efficient Enantioselective Synthesis of Florfenicol Based on Sharpless Asymmetric Dihydroxylation. *Synthesis* **2012**, *44*, 699−704.

(15) Wang, X.; Xu, L.; Yan, L.; Wang, H.; Han, S.; Wu, Y.; Chen, F. Catalytic asymmetric transfer hydrogenation/dynamic kinetic reso-

lution: an efficient synthesis of florfenicol. *Tetrahedron* **2016**, *72*, 1787−1793.
(16) Zou, J.; Ni, G.; Tang, J.; Yu, J.; Jiang, L.; Ju, D.; Zhang, F.; Chen, S. Asymmetric Synthesis of Florfenicol by Dynamic Reductive Kinetic Resolution with Ketoreductases. *Eur. J. Org. Chem.* **2018**, *2018*, 5044−5053.
(17) Fryszkowska, A.; Devine, P. N. Biocatalysis in drug discovery and development. *Curr. Opin. Chem. Biol.* **2020**, *55*, 151−160.
(18) Wu, S.; Snajdrova, R.; Moore, J. C.; Baldenius, K.; Bornscheuer, U. T. Biocatalysis: Enzymatic Synthesis for Industrial Applications. *Angew. Chem., Int. Ed.* **2021**, *60*, 88−119.
(19) Sheldon, R. A.; Pereira, P. C. Biocatalysis engineering: the big picture. *Chem. Soc. Rev.* **2017**, *46*, 2678−2691.
(20) Su, B.; Xu, L.; Xu, X.; Wang, L.; Li, A.; Lin, J.; Ye, L.; Yu, H. Redesign of a short-chain dehydrogenase/reductase for asymmetric synthesis of ethyl (R)-2-hydroxy-4-phenylbutanoate based on per-residue free energy decomposition and sequence conservatism analysis. *Green Synth. Catal.* **2020**, *1*, 150−159.
(21) Li, J.; Qu, G.; Shang, N.; Chen, P.; Men, Y.; Liu, W.; Mei, Z.; Sun, Y.; Sun, Z. Near-perfect control of the regioselective glucosylation enabled by rational design of glycosyltransferases. *Green Synth. Catal.* **2021**, *2*, 45−53.
(22) Steinreiber, J.; Fesko, K.; Reisinger, C.; Schürmann, M.; van Assema, F.; Wolberg, M.; Mink, D.; Griengl, H. Threonine aldolases—an emerging tool for organic synthesis. *Tetrahedron* **2007**, *63*, 918−926.
(23) Liu, Z.; Chen, X.; Chen, Q.; Feng, J.; Wang, M.; Wu, Q.; Zhu, D. Engineering of l-threonine aldolase for the preparation of 4-(methylsulfonyl)phenylserine, an important intermediate for the synthesis of florfenicol and thiamphenicol. *Enzyme Microb. Technol.* **2020**, *137*, 109551.
(24) Zheng, W.; Yu, H.; Fang, S.; Chen, K.; Wang, Z.; Cheng, X.; Xu, G.; Yang, L.; Wu, J. Directed Evolution of L-Threonine Aldolase for the Diastereoselective Synthesis of β-Hydroxy-α-amino Acids. *ACS Catal.* **2021**, 3198−3205.
(25) Xu, L.; Wang, L.-C.; Xu, X.-Q.; Lin, J. Characteristics of L-threonine transaldolase for asymmetric synthesis of β-hydroxy-α-amino acids. *Catal. Sci. Technol.* **2019**, *9*, 5943−5952.
(26) Xu, L.; Wang, L. C.; Su, B. M.; Xu, X. Q.; Lin, J. Multi-enzyme cascade for improving β-hydroxy-α-amino acids production by engineering L-threonine transaldolase and combining acetaldehyde elimination system. *Bioresour. Technol.* **2020**, *310*, 123439.
(27) Li, Q.; Zhang, H.; Li, C.; Xu, P. Stereoselective Synthesis of (−)-Chloramphenicol, (+)-Thiamphenicol and (+)-Sphinganine via Chiral Tricyclic Iminolactone. *Chin. J. Chem.* **2013**, *31*, 149−153.
(28) Ingram, C. U.; Bommer, M.; Smith, M. E. B.; Dalby, P. A.; Ward, J. M.; Hailes, H. C.; Lye, G. J. One-pot synthesis of amino-alcohols using a de-novo transketolase and β-alanine: pyruvate transaminase pathway in *Escherichia coli*. *Biotechnol. Bioeng.* **2007**, *96*, 559−569.
(29) Sehl, T.; Maugeri, Z.; Rother, D. Multi-step synthesis strategies towards 1,2-amino alcohols with special emphasis on phenylpropanol-amines. *J. Mol. Catal. B: Enzym.* **2015**, *114*, 65−71.
(30) Bawn, M.; Subrizi, F.; Lye, G. J.; Sheppard, T. D.; Hailes, H. C.; Ward, J. M. One-pot, two-step transaminase and transketolase synthesis of l-gluco-heptulose from l-arabinose. *Enzyme Microb. Technol.* **2018**, *116*, 16−22.
(31) Gupta, P.; Mahajan, N. Biocatalytic approaches towards the stereoselective synthesis of vicinal amino alcohols. *New J. Chem.* **2018**, *42*, 12296−12327.
(32) Casajus, H.; Lagarde, A.; Leremboure, M.; De Dios Miguel, T.; Nauton, L.; Thery, V.; Fessner, W. D.; Duguet, N.; Charmantray, F.; Hecquet, L. Enzymatic Synthesis of Aliphatic Acyloins Catalyzed by Thermostable Transketolase. *ChemCatChem* **2020**, *12*, 5772−5779.
(33) Hailes, H. C.; Rother, D.; Müller, M.; Westphal, R.; Ward, J. M.; Pleiss, J.; Vogel, C.; Pohl, M. Engineering stereoselectivity of ThDP-dependent enzymes. *FEBS J.* **2013**, *280*, 6374−6394.
(34) Saravanan, T.; Reif, M.-L.; Yi, D.; Lorillière, M.; Charmantray, F.; Hecquet, L.; Fessner, W.-D. Engineering a thermostable transketolase for arylated substrates. *Green Chem.* **2017**, *19*, 481−489.
(35) Affaticati, P. E.; Dai, S.-B.; Payongsri, P.; Hailes, H. C.; Tittmann, K.; Dalby, P. A. Structural Analysis of an Evolved Transketolase Reveals Divergent Binding Modes. *Sci. Rep.* **2016**, *6*, 35716.
(36) Galman, J. L.; Steadman, D.; Bacon, S.; Morris, P.; Smith, M. E. B.; Ward, J. M.; Dalby, P. A.; Hailes, H. C. α,α'-Dihydroxyketone formation using aromatic and heteroaromatic aldehydes with evolved transketolase enzymes. *Chem. Commun.* **2010**, *46*, 7608.
(37) Kochetov, G. A.; Solovjeva, O. N. Structure and functioning mechanism of transketolase. *Biochim. Biophys. Acta, Proteins Proteomics* **2014**, *1844*, 1608−1618.
(38) Fedorchuk, T. P.; Khusnutdinova, A. N.; Evdokimova, E.; Flick, R.; Di Leo, R.; Stogios, P.; Savchenko, A.; Yakunin, A. F. One-Pot Biocatalytic Transformation of Adipic Acid to 6-Aminocaproic Acid and 1,6-Hexamethylenediamine Using Carboxylic Acid Reductases and Transaminases. *J. Am. Chem. Soc.* **2020**, *142*, 1038−1048.
(39) Slabu, I.; Galman, J. L.; Lloyd, R. C.; Turner, N. J. Discovery, Engineering, and Synthetic Application of Transaminase Biocatalysts. *ACS Catal.* **2017**, *7*, 8263−8284.
(40) Guo, F.; Berglund, P. Transaminase biocatalysis: optimization and application. *Green Chem.* **2017**, *19*, 333−360.
(41) Patil, M. D.; Grogan, G.; Bommarius, A.; Yun, H. Recent Advances in ω-Transaminase-Mediated Biocatalysis for the Enantioselective Synthesis of Chiral Amines. *Catalysts* **2018**, *8*, 254.
(42) Steffen-Munsberg, F.; Vickers, C.; Kohls, H.; Land, H.; Mallin, H.; Nobili, A.; Skalden, L.; van den Bergh, T.; Joosten, H.-J.; Berglund, P.; Höhne, M.; Bornscheuer, U. T. Bioinformatic analysis of a PLP-dependent enzyme superfamily suitable for biocatalytic applications. *Biotechnol. Adv.* **2015**, *33*, 566−604.
(43) Sehl, T.; Hailes, H. C.; Ward, J. M.; Wardenga, R.; von Lieres, E.; Offermann, H.; Westphal, R.; Pohl, M.; Rother, D. Two steps in one pot: enzyme cascade for the synthesis of nor(pseudo)ephedrine from inexpensive starting materials. *Angew. Chem., Int. Ed.* **2013**, *52*, 6772−6775.
(44) Erdmann, V.; Sehl, T.; Frindi Wosch, I.; Simon, R. C.; Kroutil, W. Methoxamine Synthesis in a Biocatalytic 1-Pot 2-Step Cascade Approach. *ACS Catal.* **2019**, *9*, 7380−7388.
(45) Payongsri, P.; Steadman, D.; Hailes, H. C.; Dalby, P. A. Second generation engineering of transketolase for polar aromatic aldehyde substrates. *Enzyme Microb. Technol.* **2015**, *71*, 45−52.
(46) Mitschke, L.; Parthier, C.; Schröder-Tittmann, K.; Coy, J.; Lüdtke, S.; Tittmann, K. The Crystal Structure of Human Transketolase and New Insights into Its Mode of Action. *J. Biol. Chem.* **2010**, *285*, 31559−31570.
(47) Höhne, M.; Schätzle, S.; Jochens, H.; Robins, K.; Bornscheuer, U. T. Rational assignment of key motifs for function guides in silico enzyme identification. *Nat. Chem. Biol.* **2010**, *6*, 807−813.
(48) Savile, C. K.; Janey, J. M.; Mundorff, E. C.; Moore, J. C.; Tam, S.; Jarvis, W. R.; Colbeck, J. C.; Krebber, A.; Fleitz, F. J.; Brands, J.; Devine, P. N.; Huisman, G. W.; Hughes, G. J. Biocatalytic Asymmetric Synthesis of Chiral Amines from Ketones Applied to Sitagliptin Manufacture. *Science* **2010**, *329*, 305−309.
(49) Bea, H.-S.; Park, H.-J.; Lee, S.-H.; Yun, H. Kinetic resolution of aromatic β-amino acids by ω-transaminase. *Chem. Commun.* **2011**, *47*, 5894.
(50) Weiß, M. S.; Pavlidis, I. V.; Spurr, P.; Hanlon, S. P.; Wirz, B.; Iding, H.; Bornscheuer, U. T. Amine Transaminase Engineering for Spatially Bulky Substrate Acceptance. *ChemBioChem* **2017**, *18*, 1022−1026.
(51) Koszelewski, D.; Lavandera, I.; Clay, D.; Rozzell, D.; Kroutil, W. Asymmetric Synthesis of Optically Pure Pharmacologically Relevant Amines Employing ω-Transaminases. *Adv. Synth. Catal.* **2008**, *350*, 2761−2766.
(52) Andrade, L. H.; Silva, A. V.; Milani, P.; Koszelewski, D.; Kroutil, W. ω-Transaminases as efficient biocatalysts to obtain novel

https://doi.org/10.1021/acscatal.1c01229
ACS Catal. 2021, 11, 7477−7488

chiral selenium-amine ligands for Pd-catalysis. *Org. Biomol. Chem.* **2010**, *8*, 2043.
(53) Wang, B.; Land, H.; Berglund, P. An efficient single-enzymatic cascade for asymmetric synthesis of chiral amines catalyzed by ω-transaminase. *Chem. Commun.* **2013**, *49*, 161−163.
(54) Ryan, J.; Šiaučiulis, M.; Gomm, A.; Maciá, B.; O'Reilly, E.; Caprio, V. Transaminase Triggered Aza-Michael Approach for the Enantioselective Synthesis of Piperidine Scaffolds. *J. Am. Chem. Soc.* **2016**, *138*, 15798−15800.
(55) O'Reilly, E.; Iglesias, C.; Ghislieri, D.; Hopwood, J.; Galman, J. L.; Lloyd, R. C.; Turner, N. J. A Regio- and Stereoselective ω-Transaminase/Monoamine Oxidase Cascade for the Synthesis of Chiral 2,5-Disubstituted Pyrrolidines. *Angew. Chem., Int. Ed.* **2014**, *53*, 2447−2450.
(56) Cheng, F.; Li, J. M.; Zhou, S. P.; Liu, Q.; Jin, L. Q.; Xue, Y. P.; Zheng, Y. G. A Single-Transaminase-Catalyzed Biocatalytic Cascade for Efficient Asymmetric Synthesis of l-Phosphinothricin. *ChemBioChem* **2021**, *22*, 345−348.
(57) Romney, D. K.; Murciano-Calles, J.; Wehrmüller, J. E.; Arnold, F. H. Unlocking Reactivity of TrpB: A General Biocatalytic Platform for Synthesis of Tryptophan Analogues. *J. Am. Chem. Soc.* **2017**, *139*, 10769−10776.
(58) Chen, C. S.; Fujimoto, Y.; Girdaukas, G.; Sih, C. J. Quantitative analyses of biochemical kinetic resolutions of enantiomers. *J. Am. Chem. Soc.* **1982**, *104*, 7294−7299.
(59) Yilmaz, E.; Can, K.; Sezgin, M.; Yilmaz, M. Immobilization of Candida rugosa lipase on glass beads for enantioselective hydrolysis of racemic Naproxen methyl ester. *Bioresour. Technol.* **2011**, *102*, 499−506.
(60) Han, S. W.; Kim, J.; Cho, H. S.; Shin, J. S. Active Site Engineering of ω-Transaminase Guided by Docking Orientation Analysis and Virtual Activity Screening. *ACS Catal.* **2017**, *7*, 3752−3762.
(61) Voss, M.; Das, D.; Genz, M.; Kumar, A.; Kulkarni, N.; Kustosz, J.; Kumar, P.; Bornscheuer, U. T.; Höhne, M. In Silico Based Engineering Approach to Improve Transaminases for the Conversion of Bulky Substrates. *ACS Catal.* **2018**, *8*, 11524−11533.
(62) Radisky, E. S.; Koshland, D. E. A clogged gutter mechanism for protease inhibitors. *Proc. Natl. Acad. Sci. U. S. A.* **2002**, *99*, 10316−10321.
(63) Zheng, W.; Chen, K.; Wang, Z.; Cheng, X.; Xu, G.; Yang, L.; Wu, J. Construction of a Highly Diastereoselective Aldol Reaction System with l-Threonine Aldolase by Computer-Assisted Rational Molecular Modification and Medium Engineering. *Org. Lett.* **2020**, *22*, 5763−5767.
(64) Eliot, A. C.; Kirsch, J. F. Pyridoxal Phosphate Enzymes: Mechanistic, Structural, and Evolutionary Considerations. *Annu. Rev. Biochem.* **2004**, *73*, 383−415.
(65) Salomon-Ferrer, R.; Götz, A. W.; Poole, D.; Le Grand, S.; Walker, R. C. Routine Microsecond Molecular Dynamics Simulations with AMBER on GPUs. 2. Explicit Solvent Particle Mesh Ewald. *J. Chem. Theory Comput.* **2013**, *9*, 3878−3888.
(66) Maier, J. A.; Martinez, C.; Kasavajhala, K.; Wickstrom, L.; Hauser, K. E.; Simmerling, C. ff14SB: Improving the Accuracy of Protein Side Chain and Backbone Parameters from ff99SB. *J. Chem. Theory Comput.* **2015**, *11*, 3696−3713.
(67) Berendsen, H. J. C.; Postma, J. P. M.; van Gunsteren, W. F.; DiNola, A.; Haak, J. R. Molecular dynamics with coupling to an external bath. *J. Chem. Phys.* **1984**, *81*, 3684−3690.
(68) Darden, T.; York, D.; Pedersen, L. Particle mesh Ewald: An N·log(N) method for Ewald sums in large systems. *J. Chem. Phys.* **1993**, *98*, 10089−10092.
(69) Roe, D. R.; Cheatham, T. E., III PTRAJ and CPPTRAJ: Software for Processing and Analysis of Molecular Dynamics Trajectory Data. *J. Chem. Theory Comput.* **2013**, *9*, 3084−3095.

https://doi.org/10.1021/acscatal.1c01229
ACS Catal. 2021, 11, 7477−7488